Macromolecular Bioscience
www.mbs-journal.de

Innovative Fluorescent Polymers in Niosomal Carriers: A Novel Approach to Enhancing Cancer Therapy and Imaging

*Selay Tornaci, Merve Erginer, Umut Bulut, Beste Sener, Elifsu Persilioglu, İsmail Bergutay Kalaycilar, Emine Guler Celik, Hasret Yardibi, Pinar Siyah, Oguzhan Karakurt, Ali Cirpan, Baris Gokalsin, Ahmet Murat Senisik, and Firat Baris Barlas**

Cancer is anticipated to become the pioneer reason of disease-related deaths worldwide in the next two decades, underscoring the urgent need for personalized and adaptive treatment strategies. These strategies are crucial due to the high variability in drug efficacy and the tendency of cancer cells to develop resistance. This study investigates the potential of theranostic nanotechnology using three innovative fluorescent polymers (FP-1, FP-2, and FP-3) encapsulated in niosomal carriers, combining therapy (chemotherapy and radiotherapy) with fluorescence imaging. These cargoes are assessed for their cytotoxic effects across three cancer cell lines (A549, MCF-7, and HOb), with further analysis to determine their capacity to augment the effects of radiotherapy using a Linear Accelerator (LINAC) at specific doses. Fluorescence microscopy is utilized to verify their uptake and localization in cancerous versus healthy cell lines. The results confirmed that these niosomal cargoes not only improved the antiproliferative effects of radiotherapy but also demonstrate the practical application of fluorescent polymers in in vitro imaging. This dual function underscores the importance of dose optimization to maximize therapeutic benefits while minimizing adverse effects, thereby enhancing the overall efficacy of cancer treatments.

1. Introduction

Cancer continues to pose a formidable challenge to global health, firmly established as the second pioneer cause of mortality worldwide. The Global Cancer Observatory's data for 2020 indicates a daunting figure of 19.3 million new cases and nearly 10 million deaths, highlighting a particularly alarming prevalence of lung cancer among males in Turkey, almost double the global average.[1] The complete and effective control of cancer treatment can only be achieved through a dynamic, multidimensional, scientific, multidisciplinary, and cost-effective program. Failure to take necessary measures against cancer and implement a systematic control program is expected to result in costs exceeding healthcare budgets in many countries in the coming years.[2]

The utilization of a single strategy in cancer treatment is acknowledged to be

S. Tornaci
Department of Bioengineering
Faculty of Enginering
Marmara University
Istanbul 34722, Turkey

M. Erginer, F. B. Barlas
Institute of Nanotechnology and Biotechnology
Istanbul Univeristy-Cerrahpasa
Istanbul 34500, Turkey
E-mail: fbbarlas@iuc.edu.tr

M. Erginer, F. B. Barlas
Health Biotechnology Joint Research and Applications Center of Excellence
Istanbul 34220, Turkey

U. Bulut
Faculty of Pharmacy, Department of Analytical Chemistry
Acıbadem Mehmet Ali Aydınlar University
Istanbul 34752, Turkey

B. Sener, B. Gokalsin
Department of Biology, Faculty of Science
Marmara University
Istanbul 34722, Turkey

E. Persilioglu
Department of Biochemistry, School of Medicine
Bahcesehir University
Istanbul 34734, Turkey

İ. B. Kalaycilar, H. Yardibi
Department of Biochemistry, Faculty of Veterinary Medicine
Istanbul University-Cerrahpasa
Istanbul 34500, Turkey

The ORCID identification number(s) for the author(s) of this article can be found under https://doi.org/10.1002/mabi.202400343

DOI: 10.1002/mabi.202400343

insufficient due to: i) the significant side effects commonly associated with such approaches, ii) the variability in treatment outcomes among different individuals, and iii) the high resistance capabilities of cancer cells. Theranostic treatments, which combine therapeutic and diagnostic capabilities in a single platform, represent a significant advancement in personalized medicine. These systems are designed to diagnose, deliver targeted therapy, and monitor the response to treatment simultaneously, increasing the efficacy and safety of medical interventions. Recent developments in nanotechnology have significantly enhanced the potential of theranostics, particularly using nanoparticles capable of carrying both imaging agents and therapeutic drugs. For example, nanoparticles can be designed to target cancer cells explicitly by being coated with specific ligands, deliver therapeutic payloads, and concurrently allow for real-time imaging of the drug's distribution and effect. These multifunctional nanoparticles provide opportunities for early tumor detection and evaluation of therapeutic efficacy.[3] This integrative approach not only ensures the precise delivery of therapeutics but also facilitates continuous monitoring of the treatment's effectiveness, thereby optimizing patient outcomes.[4]

Radiotherapy is a treatment method that aims to destroy or inhibit the growth of cancer cells by using high-energy radiation. It is typically administered using types of radiation such as X-rays, gamma rays, or protons. Radiotherapy works by damaging the DNA of cancer cells, thereby preventing their proliferation, and spread.[5] Radiotherapy is one of the most widely used non-invasive cancer treatment methods today;[6] however, it has side effects depending on the level of radiation administered.[7,8] To overcome these limitations, radiosensitivity studies and combined therapy hold significant potential. Additionally, fluorescent polymers, fluorescent nanoparticles, and MR contrast agents have been frequently utilized in recent radiotherapy studies for the applicability of theranostic treatment. This is due to their adaptability to imaging systems that do not involve radiation.[9,10]

Recent advancements in nanotechnology, particularly in the integration of nanomaterials with cancer therapeutics, have spotlighted fluorescence imaging due to its non-invasiveness and enhanced contrast capabilities. These capabilities are significantly bolstered by the development of high-fluorescence polymers and nano-carrier systems.[11,12] The enhancement of biocompatibility through polymer conjugation, using substances such as Poly(amidoamine) (PAMAM),[13] Polyethylene glycol (PEG)[14] and dextran,[15] has facilitated tissue-specific drug targeting. These advancements have intensified the therapeutic effects of radiotherapy and photodynamic therapy and provided unique opportunities for precision imaging.[16–20] Conjugated polymers, based on π-electron systems, offer distinct chemical, electronic, and photophysical advantages, including high molar absorptivity and excellent photostability.[19,20] These properties make them ideal for bio-imaging applications where they mimic the properties of metals and semiconductors, maintaining traditional polymer benefits like ease of synthesis and potential for chemical modification.[21–23]

The concept of donor-acceptor (D-A) conjugate polymers, introduced by Wynberg et al. in 1992, involves the synthesis of polymers alternating between electron-rich (donor) and electron-poor (acceptor) units, typically resulting in a narrow bandgap adjustable through modifications of the donor and acceptor units.[24] Adjustments to the HOMO-LUMO gap, facilitated by extending π-conjugation or attaching large substituents to the donor segment, have pushed absorption and emission properties into the near-infrared (NIR) region, enhancing their application in NIR imaging.[25]

Niosomes, a type of non-ionic surfactant-based vesicles, represent another innovative approach in the realm of cancer therapeutics, mirroring the advancements seen in polymer technology. These vesicles are renowned for their superior stability, reduced toxicity, and cost-effectiveness compared to traditional liposomes. Such attributes make niosomes an effective drug delivery system that aligns well with biological systems, enhances bloodstream circulation time, and facilitates controlled release and targeted therapy. The versatility of niosomes has been highlighted in recent studies, which demonstrate their capability to enhance the efficacy of drug molecules through strategies such as delayed clearance and selective targeting to affected cells.[26] Further developments in noisome design and synthesis have expanded their application scope to include both topical and brain-targeted delivery, addressing critical needs in treating brain tumors and neurodegenerative diseases. Ongoing advancements in niosome-ligand conjugation are expected to provide breakthrough solutions for overcoming physiological barriers like the blood-brain barrier, thereby improving the bioavailability of therapeutic agents.[27]

In addition to their role in systemic drug delivery, niosomes are being explored for transdermal drug delivery systems, exploiting their property of enhanced drug penetration and local depot formation for sustained release.[28] These carriers are apt for various administration routes, including ocular, transdermal, and central nervous system targeting, presenting a promising future for pharmaceutical applications.[29] The rise of provesicular approaches, such as proniosomes, has further widened the scope and versatility of niosomes. Nevertheless, there is a consensus that more dedicated research is necessary to fully realize their clinical potential. As a cost-effective and chemically stable option for drug delivery, niosomes stand at the forefront of nanocarrier technology, potentially enhancing the treatment efficacy for cancer and beyond.[29,30] Thus, as cancer treatment approaches a critical juncture, where traditional methods fall short, the integration of theranostic strategies that incorporate both diagnostics and therapeutics becomes paramount. This paper will explore the use

E. G. Celik
Department of Bioengineering, Faculty of Engineering
Ege University
Bornova, Izmir 35100, Turkey
P. Siyah
Department of Biochemistry, Faculty of Pharmacy
Bahçeşehir University
Istanbul 34353, Turkey
O. Karakurt, A. Cirpan
Department of Chemistry
Middle East Technical University (METU)
Ankara 06800, Turkey
A. M. Senisik
Vocational School of Health Services
Altınbas University
Istanbul 34217, Turkey

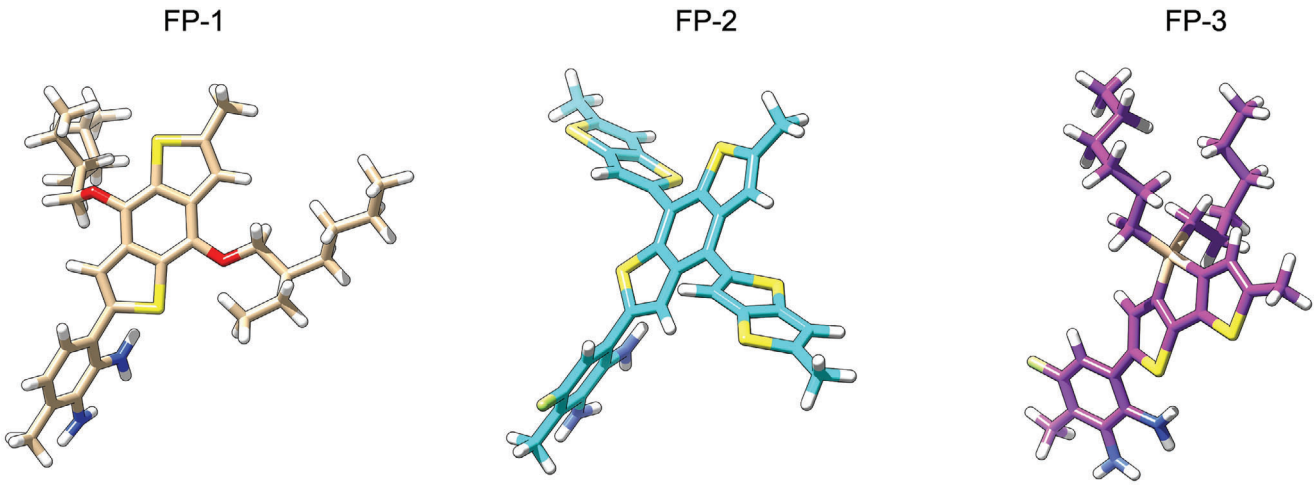

Figure 1. 3D representations of the monomer structures of FP-1, FP-2, and FP-3 polymers. Visualized in Chimera software.

of fluorescent polymer-conjugated niosomes as a promising theranostic platform, potentially redefining cancer diagnostics and personalized therapy.

Here, three fluorescent polymers (FP-1, FP-2, and FP-3) with high potential for theranostic cancer treatment were investigated for the 1 time (**Figure 1**). Initially, fluorescent polymers were utilized to form niosomal cargos, followed by characterization analyses. Subsequently, viability assays were conducted over 24, 48, and 72 h to examine the interactions of the synthesized niosomes with three different cell lines (A549, MCF-7, and HOb). The niosomal cargos exhibited cytotoxic effects at specific doses. Their potential to enhance radiotherapy was tested using a Linear Accelerator (LINAC) at 4 Gray, 6 MeV. To assess their imaging capabilities, fluorescent microscopy was employed to capture images, determine intracellular uptake, and localize their positions within cells. Finally, molecular simulation studies of the monomers of these polymers were performed to determine their affinity for MCL-1 proteins, which play a critical role in cancer treatment (Figures S1 and S2, Supporting Information).

2. Experimental Section

Chemicals were supplied from Tokyo Chemical Industry (TCI) and Merck unless otherwise mentioned. All reactions were performed under a nitrogen atmosphere. Dry solvents were obtained from a solvent drying system (Mbraun MBSPS5) and then degassed with nitrogen and 4 Å molecular sieves for 2 days. Bruker Spectrospin Avance DPX-400 Spectrometer (400 MHz) was used to obtain nuclear magnetic resonance (NMR) spectrums for structural characterizations. To determine the molecular weights of target polymers, gel permeation chromatography (GPC) (Shimadzu RID-20A with polystyrene standard) was used.

2.1. Synthesis and Characterization of Fluorescent Polymers

2.1.1. Synthesis of Monomers

The synthetic pathway to obtain **M1** (3,6-dibromo −1,2-diamine) and **M2** (3,6-dibromo-4-fluorobenzene-1,2-diamine) is shown in **Figure 2**. All compounds were synthesized according to reported procedures in the literature.[31,32] To synthesize molecule **2** (5-fluorobenzo[c][1,2,5] thiadiazole), commercially available 4-fluoro-2-nitroaniline was reduced by using tin (Sn) and hydrochloric acid (HCl) at 0 °C and the intermediate (4-fluorobenzene-1,2-diamine) was successfully obtained with a high yield. Because the intermediate immediately decomposes in the open air, it was directly used without purification. After that, a ring closure reaction using thionyl chloride ($SOCl_2$) and triethyl amine was performed, and molecule **3** was successfully obtained in a total yield of 70%. To obtain molecules **1** (4,7-dibromo benzo[*c*][1,2,5] thiadiazole) and **4** (4,7-dibromo-5-fluorobenzo[*c*][1,2,5] thiadiazole), a bromination reaction with molecular bromine (Br_2) and hydrobromic acid (HBr) was performed. Molecules **1** and **2** were successfully obtained with a moderate yield of ≈52%. Finally, the target molecules (**M1** and **M2**) were synthesized by reduction

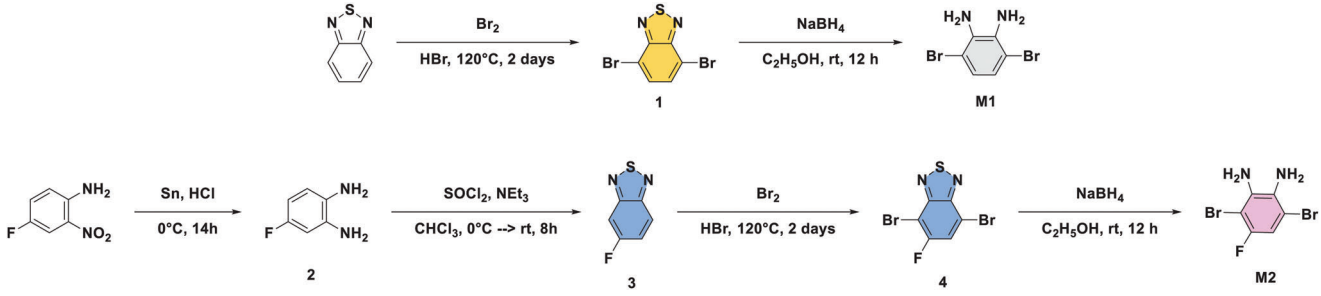

Figure 2. Synthetic pathway to obtain monomers **1** and **2**.

reaction using sodium borohydride ($NaBH_4$) with a high yield. Similar to the previous intermediate (4-fluorobenzene-1,2-diamine), monomers also decompose quickly in open air; hence, it was directly used for polymerization reaction without any purification. The NMR spectrum of the final isolated compound (molecule **4**) was obtained and provided in Figure S4 (Supporting Information). ^{1}H NMR (400 MHz, $CDCl_3$) δ 7.79 (d, J = 8.3 Hz, 1H).

2.1.2. Synthesis of Fluorescent Polymers

Synthesis of FP-1: FP-1 is synthesized through the reaction of 4,8-bis((2-ethylhexyl)oxy)benzo[1,2-b:4,5-b']dithiophene-2,6-diyl)bis(trimethyltin) with 3,6-dibromobenzene-1,2-diamine in the presence of $Pd(PPh_3)_2Cl_2$ as described in our previous work.[33] Detailed visualization is provided in Figure S3 (Supporting Information).

Synthesis of FP-2: In a 25 mL Schlenk tube, 57.0 mg **D1** (200.76 µmol), 149.44 mg **A1** (200.76 µmol), and 6.0 mg tri(o-tolyl)phosphine ($(CH_3C_6H_4)_3P$) (20.08 µmol) were added. The Schlenk tube was vacuumed for 30 min, and then argon gas was allowed to pass through the Schlenk tube to remove possible oxygen and humidity residues. This process was repeated 3 times. 4 mL of dry toluene ($C_6H_5CH_3$) was added under an argon atmosphere, and the mixture temperature was set to 60 °C. The mixture was degassed for 1 h. Then 4.00 mg tris(dibenzylideneacetone)dipalladium(0) ($Pd_2(dba)_3$) (6.96 µmol) were added to the reaction mixture, and the temperature was set to 100 °C. The reaction was refluxed for 72 h. Then, 2-stanyllatedthiophene was added to the reaction mixture, and after 3 h, 2-bromothiophene was added, and the reaction was refluxed overnight. The reaction mixture was poured into the cold MeOH and precipitated. Then, 50 mg of palladium scavenger (3-(Diethylenetriamine)propyl-functionalized silica gel) was added and stirred for 1 h. The crude polymer was then filtrated and collected. The crude polymer was washed with Soxhlet apparatus with an order of methanol, acetone and hexane. Hexane fragment was collected. Hexane was evaporated under reduced pressure, and red **FP-2** was collected (67 mg, 58% yield). GPC Result: Mn = 5.9 kDa, Mw = 10.1 kDa PDI = 1.71. As expected, the ^{1}H NMR spectrum of the polymer displayed broad bands in both aromatic and aliphatic regions. ^{1}H NMR (400 MHz, $CDCl_3$, δ: ppm) 8.00–7.00 (aromatic region), 2.00–0.50 (aliphatic region). Detailed visualization is provided in Figure S3 (Supporting Information).

Synthesis of FP-3: In a 25 mL Schlenk tube 50.0 mg **D2** (176.10 µmol), 179.05 mg **A1** (176.10 µmol), and 5.0 mg tri(o-tolyl)phosphine ($(CH_3C_6H_4)_3P$) (17.61 µmol) were added. The Schlenk tube was vacuumed for 30 min. then, argon gas was allowed to pass through the Schlenk tube to remove possible oxygen and humidity residues. This process was repeated 3 times. 4 mL of dry toluene ($C_6H_5CH_3$) was added under an argon atmosphere, and the mixture temperature was set to 60 °C. The mixture was degassed for 1 h. Then 5.00 mg tris(dibenzylideneacetone)dipalladium(0) ($Pd_2(dba)_3$) (5.46 µmol) were added to the reaction mixture, and the temperature was set to 100 °C. The reaction was refluxed for 72 h. Then, 2-stanyllatedthiophene was added to the reaction mixture, and after 3 h, 2-bromothiophene was added, and the reaction was refluxed overnight. The reaction mixture was poured into the cold MeOH and precipitated. Then, 50 mg of palladium scavenger (3-(Diethylenetriamine)propyl-functionalized silica gel) was added and stirred for 1 h. The crude polymer was then filtrated and collected. The crude polymer was washed with Soxhlet apparatus with an order of methanol, acetone and hexane. Hexane fragment was collected. Hexane was evaporated under reduced pressure, and red **FP-3** was collected (32 mg, 21.55% yield). GPC Result: M_n = 3.5 kDa, Mw = 6.1 kDa PDI = 1.74 ^{1}H NMR (400 MHz, $CDCl_3$, δ: ppm) 8.20–6.90 (aromatic region), 3.00–0.35 (aliphatic region). Detailed visualization is provided in Figure S3 (Supporting Information).

2.2. Encapsulation and Characterization of Fluorescent Polymers in Niosomes

2.2.1. Niosome Synthesis

Niosomes were prepared using the thin-film hydration method with ultrasonication.[34] A mixture of Tween 61, cholesterol, and polymers in a 1:1:0.1 ratio was dissolved in chloroform and methanol (2:1 mL) in a round-bottom flask. The solvent was then evaporated using a rotary evaporator (Buchi R-3, Switzermttland) to form a thin film, which was left overnight in a vacuum desiccator. The following day, 5 mL of PBS was added and vortexed over the thin film, creating a solution containing macro and microvesicles. The solution was then passed through filters using a mini extruder (Avanti) to reduce vesicle size to the nano level. Finally, the resulting niosomes were dialyzed against PBS to remove unconjugated and/or unencapsulated polymers.

2.2.2. Characterization Analyses

Entrapment Efficiency (EE): Dialysis against PBS was performed to remove unentrapped FP-1, FP-2, and FP-3. The entrapped polymers were quantified by completely dissolving the vesicles in chloroform and spectrophotometrically analyzing the solution at 370, 400, and 410 nm using a Thermo plate reader, alongside a calibration curve. Entrapment efficiency (EE%) was calculated as (Amount Retained / Total Amount) × 100. Each synthesis was repeated 3 times at different times to ensure consistent characterization results. The size of the encapsulated niosomes was analyzed using Dynamic Light Scattering (DLS) with a Malvern Zetasizer Nano ZS model, and Scanning Electron Microscopy (SEM) was performed.

DLS and Zeta Potential Analyses: Size and zeta potential analyses of the niosomal cargos were conducted using a Malvern Zetasizer device.

SEM Analysis: SEM analyses were carried out using a Thermo Fisher Quattro S to assess the size of the niosomal cargos.

2.2.3. Determining the Efficacy of Developed Theranostic Nanocarriers In Vitro

Cell Culture Studies: Cancerous human breast epithelial cell line (MCF-7) and human lung adenocarcinoma cell line (A549),

as well as healthy human bone cell line (HOb), were cultured in Dulbecco's Modified Eagle Medium (DMEM) and Minimum Essential Medium (MEM) supplemented with L-Glutamine, 10% fetal bovine serum (FBS), and 10000 U mL^{-1} each of penicillin and streptomycin (all from Lonza, Switzerland). Cultures were maintained at 37 °C in a 5% CO2, 95% humidity environment and passaged twice weekly.

Cell Viability Test (MTT): The MTT assay was conducted as previously described[10] MTT, a tetrazolium salt, is metabolized by live cell mitochondria to form insoluble purple formazan, which accumulates intracellularly. 4×10^3 Cells were seeded in 96-well plates and incubated under normal conditions for 48 h. After removing the old medium, various concentrations of treatment medium were added. Post-treatment, 110 µL of a 5.0 mg mL^{-1} MTT solution in PBS was added to each well for a 4 h incubation, after which 100 µL of SDS was used to dissolve the formazan crystals. Plates were incubated for 24 h, and absorbance was measured at 570 nm with a 630 nm reference.[10]

Radiotherapy Studies: Two experimental groups were set up: one to determine if fluorescent polymers enhance radiotherapy and another for in vitro gene expression of apoptosis. 4×10^3 Cells were seeded in 96-well plates and incubated overnight. Non-toxic concentrations of empty niosomes or niosomes containing FP-1, FP-2, and FP-3 were added, followed by a 2 h incubation. Cells were then exposed to 4 Gy radiation using a linear accelerator (Elekta Versa HD). Post-radiation, cells were incubated at 37 °C and 5% CO^2 for 72 h, and cell viability was assessed using the MTT assay.

Use in Fluorescence Imaging Studies: Cells from cancerous and healthy lines were seeded in 8-well chamber slides (4×10^3 cells/per well) and incubated for 2 days. Following incubation, the cells were exposed to media containing the sample for 2 h, then rinsed 3 times with PBS, and stained with DAPI for 15 min. Fluorescence microscopy was used to capture images with red and DAPI filters, and the results were compared to those of the control groups.[35]

2.2.4. Assessment of Apoptosis via In Vitro Gene Expression Analysis

Three cell lines were seeded into 15 75 cm^2 culture flasks and incubated for 2 days until they reached 80% confluency. Five groups were established for each cell line: a non-irradiated control group, an irradiated group without niosomal cargo treatment, and irradiated groups treated with niosomal cargos containing FP-1, FP-2, or FP-3 polymers. The groups were treated with non-toxic doses of niosomal cargos and incubated for 2 h for cellular uptake. Following this, the cells were exposed to 4 Gray of radiation using a LINAC system. Total RNA was isolated using Tripure (Roche, Sweden) and converted to cDNA using the Firescript RT cDNA Synthesis Kit (Solis Biodyne, Estonia).[36,37] Real-time PCR was performed with gene-specific primers for β-actin, Caspase 3, and Caspase 9, synthesized by SENTE BIOLAB (Ankara, Turkey), and SYBR Green Master Mix on a LightCycler 96 system (Roche, Sweden). Gene expression was normalized to β-actin, and PCR reactions were performed in triplicate. Results were analyzed with The LightCycler 96 System Software (Roche) to calculate melting temperatures and threshold cycles (Ct), with gene expression changes compared using logarithmic (log 2) graphs.

2.2.5. Statistical Analysis

Results were presented as mean ± SD (standard deviation). Statistical analysis was performed using one-way ANOVA, followed by Tukey's multiple comparisons test with GraphPad Prism 9 software. A p-value of <0.01 was considered statistically significant.

3. Results and Discussion

3.1. Fluorescent Polymers

The polymers used in this study incorporate benzodithiophene and silolodithiophene units to improve thermal stability and have been functionalized to enhance targeting and imaging capabilities. Additionally, amino functional groups were introduced to enable the modification of polymers with targeting and/or imaging agents. Among the polymers, FP-1 has previously been used in sensor studies aimed for testosterone analysis (25), while FP-2 and FP-3 were specifically synthesized for this study, and all three polymers were tested for the 1 time for cancer diagnosis and treatment. Polymerization reactions were conducted via Stille cross-coupling reactions, and polymers were characterized via 1H NMR spectroscopy and GPC.[31,32,33,38] NMR spectra of the polymers are provided in Figure S4 (Supporting Information).

This study focuses on nanovesicular-based carrier systems, which are increasingly utilized across a variety of biological applications, including drug delivery, imaging, and diagnostics. The functional capacity of these systems is critically dependent on parameters such as nanoparticle size, surface charge, and encapsulation efficiency. The dimension of nanoparticles is pivotal, influencing their ability to target and be internalized by cells, with optimal size ranges enhancing membrane penetration, circulation duration, and uptake efficiency.

The encapsulation efficiencies of the synthesized niosomes were initially calculated using formulations for FP-1, FP-2, and FP-3 respectively as follows: $y = 0.0009x+0.0925$ ($R^2 = 0.9707$), $y = 0.0009x+0.1461$ ($R^2 = 0.959$), and $y = 0.0009x+0.1002$ ($R^2 = 0.9864$). The calculated encapsulation efficiencies were 65.27%, 66.18%, and 63.46% respectively. These efficiencies suggest that the liposomal carriers synthesized herein exhibit superior performance relative to vesicular systems documented in prior research.[39,40] Size analyses were conducted using Dynamic Light Scattering (DLS) and Scanning Electron Microscopy (SEM), with surface charge calculations also performed. DLS results indicated that the size of empty niosomes (control group) was 154.7 ± 26.88 nm (pdi: 0.780), FP-1 niosomes were 183.5 ± 37.06 nm (pdi: 0.724), FP-2 niosomes were 179.1 ± 29.33 nm (pdi: 1.00), and FP-3 niosomes were 233.0 ± 40.17 nm (pdi: 1.00). Nanoparticles fashioned through extrusion methods demonstrated lower polydispersity indices, indicating more uniform size distribution compared to other methodologies.[41,42] Zeta potential measurements showed values of −25.64 ± 3.2 for empty niosomes, −22.15 ± 2.1 for FP-1, −22.68 ± 4 for FP-2, and −23.11 ± 1.7 for FP-3, with −19.83 ± 3.4 also measured (**Table 1**). Variations in these charges can be attributed to the presence of positive ions at the exposed ends of the entrapped polymers, further influencing the interaction dynamics within the niosomal membranes. Surface charge

Table 1. Size and zeta potential distribution of niosomes.

Name	Size [nm]	Polydispersity index (PDI)	Zeta potential [mV]
Empty niosome	154.7 ± 26.88	0.780	−22.15 ± 2.1
FP-1 niosome	183.5 ± 37.06	0.724	−22.68 ± 4
FP-2 niosome	179.1 ± 29.33	1.00	−23.11 ± 1.7
FP-3 niosome	233.0 ± 40.17	1.00	−19.83 ± 3.4

plays a significant role in the cellular internalization of nanoparticles, where negatively charged particles are often associated with higher cellular uptake than their positively charged counterparts. This trend extends to liposomes, where charged versions achieve substantially greater cellular internalization than their uncharged equivalents, underscoring the impact of surface charge on cellular uptake mechanisms.[43,44]

Examining the SEM results, the images are remarkably clear, and it is observed that the wall structures of empty niosomes are more distinct compared to those of niosomes containing FP-1, FP-2, and FP-3. This is attributed to the entrapment of the non-water-soluble polymers within the surfactant and cholesterol-based membrane system of the niosomal structure. The results indicate that the empty niosomes possess a size range of 200–300 nm, niosomes containing FP-1 have a size range of 200–250 nm, niosomes containing FP-2 have a size range of 150–250 nm, and niosomes containing FP-3 exhibit sizes ranging from 150–300 nm. (**Figure 3**). The larger size observed in SEM compared to DLS results can be attributed to the flattened structure of niosomes during the drying process required for SEM sample preparation, rather than maintaining a perfect spherical shape. Numerous parameters, such as temperature, the method used, and the encapsulated/entrapped substance, can significantly influence the size of vesicular systems. Reviewing previous studies, we can observe that vesicular systems synthesized using similar methods exhibit comparable size ranges.[45]

3.2. Cell Culture Analyses

3.2.1. Cell Viability Analyses

In vitro viability analysis using the MTT assay is currently of great interest in biomedical research due to its various advantages in polymers, drug delivery systems, tissue engineering, and biomaterial applications. This method is highly sensitive for determining cellular viability based on mitochondrial redox activity and detecting toxic effects. It is a widely accepted and actively utilized method in contemporary research. In this study, the synthesis of fluorescent polymers and their application in niosomal cargos were explored for their effects on cell viability across different cell lines (A549, MCF-7, and HOb) using MTT assay. Over 3 time intervals (24, 48, and 72 h), the study aimed to distinguish whether the synthesized cargos exerted cytotoxic or antiproliferative effects. In the study, MTT assay results were first obtained as illustrated in **Figure 4**, followed by the calculation of IC50 values using GraphPad Prism 6. The IC50 values, which represent the concentration at which 50% inhibition of cell viability is observed, were calculated for each polymer and cell line. For the A549 line, the IC50 values were 24.43 μg mL^{-1} for FP-1, 25.37 μg mL^{-1} for FP-2, and 25.82 μg mL^{-1} for FP-3. In the MCF-7 line, they were 25.89 μg mL^{-1} for FP-1, 23.69 μg mL^{-1} for FP-2, and 25.40 μg mL^{-1} for FP-3. The HOb line showed 29.51 μg mL^{-1} for FP-1, 29.45 μg mL^{-1} for FP-2, and 29.80 μg mL^{-1} for FP-3 (**Table 2**). Conductive polymers composed of conjugated π-electron systems have been shown in previous studies to self-assemble and bind to proteins in biological systems.[46] Our synthesized fluorescent polymers exhibited greater uptake in cancerous cells compared to healthy cells, as observed in fluorescent mi-

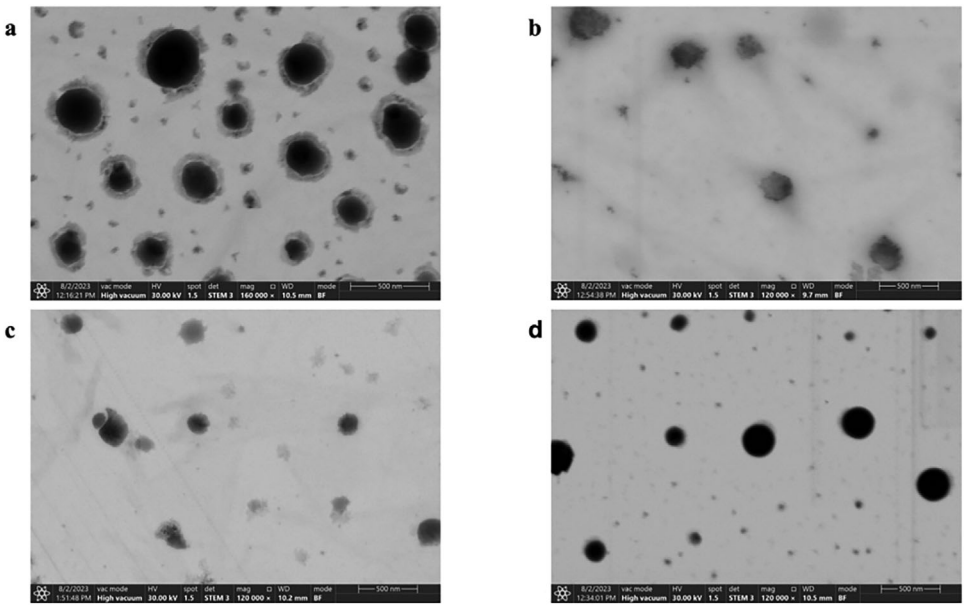

Figure 3. SEM image of niosomal kargos, a) empty niosome, b) FP-1 niosome, c) FP-2 niosome, and d) FP-3 niosome. (Scale bar: 500 nm). (High vacuum mode 30.00, HV kV).

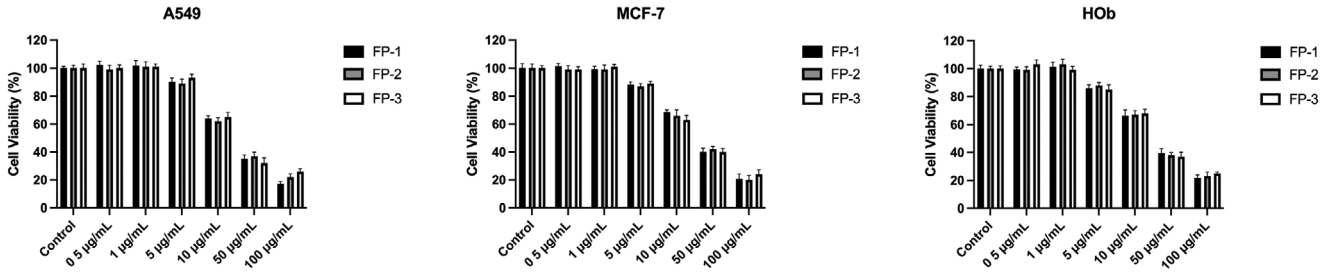

Figure 4. Cytotoxic effect of niosomal cargos (FP-1, FP-2, and FP-3) across A549, MCF-7, and HOb cell lines at 72 h.

croscopy studies. It is hypothesized that these polymers exhibit their toxic effects at high doses by binding to cytoplasmic proteins and causing a loss of their functions. Relatively non-toxic conductive polymers composed of conjugated π-electron systems have been demonstrated in various studies to be adaptable to biological systems and usable in imaging studies due to their low cytotoxicity.[47,48] Additionally, the benzodithiophene structures in the polymers we used have been shown to possess cytotoxic effects in various types of cancer.[49] A dose of 1 µg mL^{-1} was selected as the working concentration to better understand the effectiveness of subsequent analyses.

3.2.2. Radiotherapy

The rapid advancement of technology today facilitates the exploration of new methods and the improvement of existing treatments in the fight against cancer. Advanced technology allows for the testing of various strategies to combat cancer. Among these strategies, radiotherapy is widely used in clinical settings and is applied to many cancer patients. Exploring alternative methods for radiotherapy and using new materials can enhance the efficacy of cancer treatment and minimize side effects. In this context, this study examined the potential radio-enhancing effects of niosomal cargos used in the treatment. Cell lines (A549, MCF-7, and HOb) were seeded at 4×10^3 cells per well in 96-well culture plates one day prior to treatment and were exposed to 4 Gray of radiation using a clinical Linear Accelerator (LINAK). After irradiation, the cells were incubated for 72 h, followed by a viability analysis to measure changes in cell survival.

The results showed significant changes in cell viability. For the A549 cell line, viability in the control group was measured at 73.95% ± 6.65, while cells treated with niosomal cargos containing FP-1, FP-2, and FP-3 demonstrated viabilities of 40.40% ± 1.97, 60.87% ± 5.87, and 39.91% ± 2.51, respectively. In the MCF-7 cell line, control viability was 70.75% ± 2.88, compared to 45.86% ± 7.33, 57.43% ± 7.03, and 42.56% ± 7.11 for FP-1, FP-2, and FP-3 treated groups, respectively. For the HOb cell line, the control group's viability was 82.34% ± 2.99, while viabilities for cells treated with FP-1, FP-2, and FP-3 were 65.37% ± 5.41, 71.67% ± 1.56, and 64.52% ± 2.85, respectively (**Figure 5**). These analyis demonstrate the varying impacts of niosomal cargos on cell viability across different cell lines after radiation, indicating their potential use as radio-enhancers in cancer therapy.

These findings indicate that the fluorescent polymers FP-1, FP-2, and FP-3 enhanced the radiotherapeutic effects, particularly in cancerous cell lines A549 and MCF-7, with statistically significant reductions in viability (p<0.0001). However, in the healthy HOb cell line, while radiation alone caused some reduction in viability, the enhancement effects of FP-1, FP-2, and FP-3 were more limited (p<0.001). The study also notes that the inherent toxic effects of fluorescent polymers can increase the effectiveness of radiotherapy through a co-therapy effect. Literature suggests that π-electron systems in conjugated polymers can act as donor-acceptor systems, producing phototoxic effects under specific light spectra, potentially forming highly toxic nitric oxide derivatives in living systems.[50] The X-rays used in this study, emanating from a LINAK source, directly targeted the cells, supporting the potential of π-electron system polymers as radiosensitizing agents in therapy. Furthermore, the benzodithiophene structures in the polymers have been shown to exhibit cytotoxic effects on various cancer cell lines, effects that could be enhanced through external applications.[51–53] The lesser damage in HOb cells can be attributed to slower metabolism leading to lower polymer uptake and superior repair mechanisms compared to cancerous cell lines.

Table 2. IC50 values for niosomal cargos on various cell lines at 72 h.

Cell line	FP-1 [µg mL^{-1}]	FP-2 [µg mL^{-1}]	FP-3 [µg mL^{-1}]
A549	24.43	25.37	25.82
MCF-7	25.89	23.69	25.40
HOb	29.51	29.45	29.80

3.2.3. Fluorescence Microscopy

In recent years, fluorescent imaging has undergone significant evolution as an alternative to radio imaging, driven by the discovery of fluorescent nanoparticles and polymers. These technological advancements have introduced a new dimension to the application areas of theranostic treatment. Nanoparticles and polymers, particularly in the field of fluorescent imaging, have facilitated the development of advanced precision devices and offer promising potential for imaging applications. Fluorescent imaging, due to its ability to conduct detailed analyses at the cellular level, has become an important tool in biomedical research.[54] Fluorescent polymers are particularly prominent materials in theranostic applications.[55] In this study, niosomal cargos containing FP-1, FP-2, and FP-3 were applied to cell lines (4×10^3 cell/per well) cultured on chamber slides 2 days prior, followed by a 2 h incubation period. After incubation, the culture medium

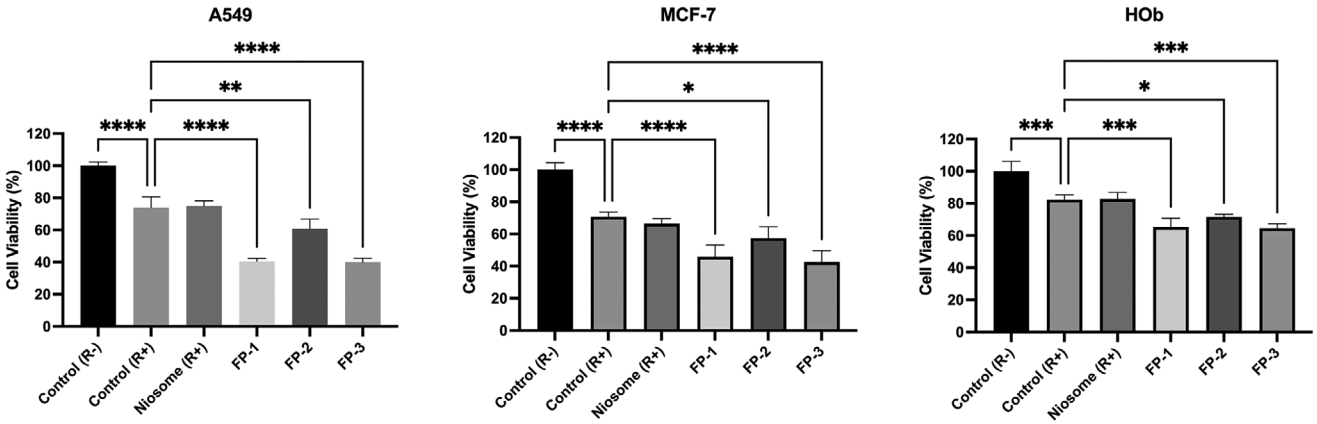

Figure 5. MTT results for combined effect of Fluorescent Polymers and Radiotherapy. (R−) mean is no radiation and (R+) mean is 4 Gy Radiation. The mean is accompanied by the standard deviation (± SD).

was removed from the cells, and PBS containing DAPI was added, followed by a 10 min incubation. Subsequently, the cells were washed 3 times with PBS, and images were captured using Texas Red (λex 596 and λem 615 nm) and DAPI filters (λex 364 nm; λem 454 nm). The images were merged using ImageJ software. According to these results, niosomal cargos containing FP-1, FP-2, and FP-3 demonstrated better retention in cancerous cell lines compared to the HOb cell line after a 2 h incubation period. This indicates a higher level of fluorescence interaction with cancerous cells, suggesting that both imaging and radiotherapy studies may demonstrate increased interaction with fluorescent polymers. No significant differences in retention were observed in the MCF-7 and A549 cell lines. Another important finding was that niosomal cargos localized within the cytoplasm of all cell lines (**Figure 6**). Similar to our study, various studies have demonstrated that conductive polymers composed of conjugated π-electron systems are adaptable to biological systems and can be used in imaging studies.[56,57] The fluorescent properties of the benzodithiophene structures in the polymers used in this study have been shown in various studies, with reports indicating their short response times.[58,59] Considering the structural characteristics of the polymers we used, it is believed that their dominant fluorescent properties are primarily due to the benzodithiophene structures. These findings underscore the targeted delivery capabilities of fluorescent polymers and their potential in theranostic applications, where their intrinsic fluorescent properties enable

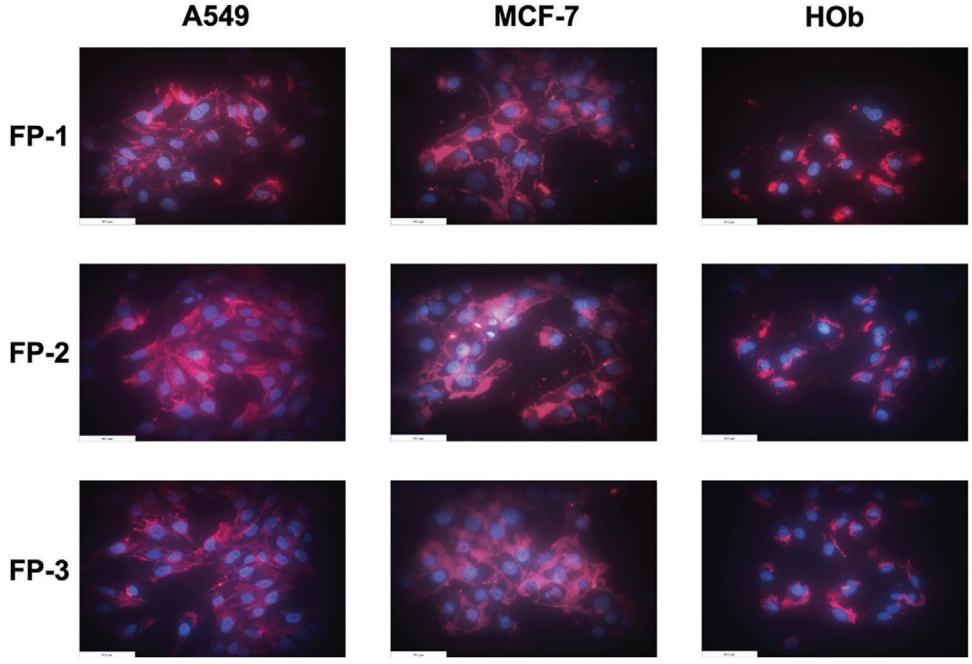

Figure 6. Fluorescence microscope images of niosomal cargo containing FP-1, FP-2, and FP-3 were obtained after 2 h incubation in A549, MCF-7, and HOb cell lines. (Scale bar: 69.2 µm).

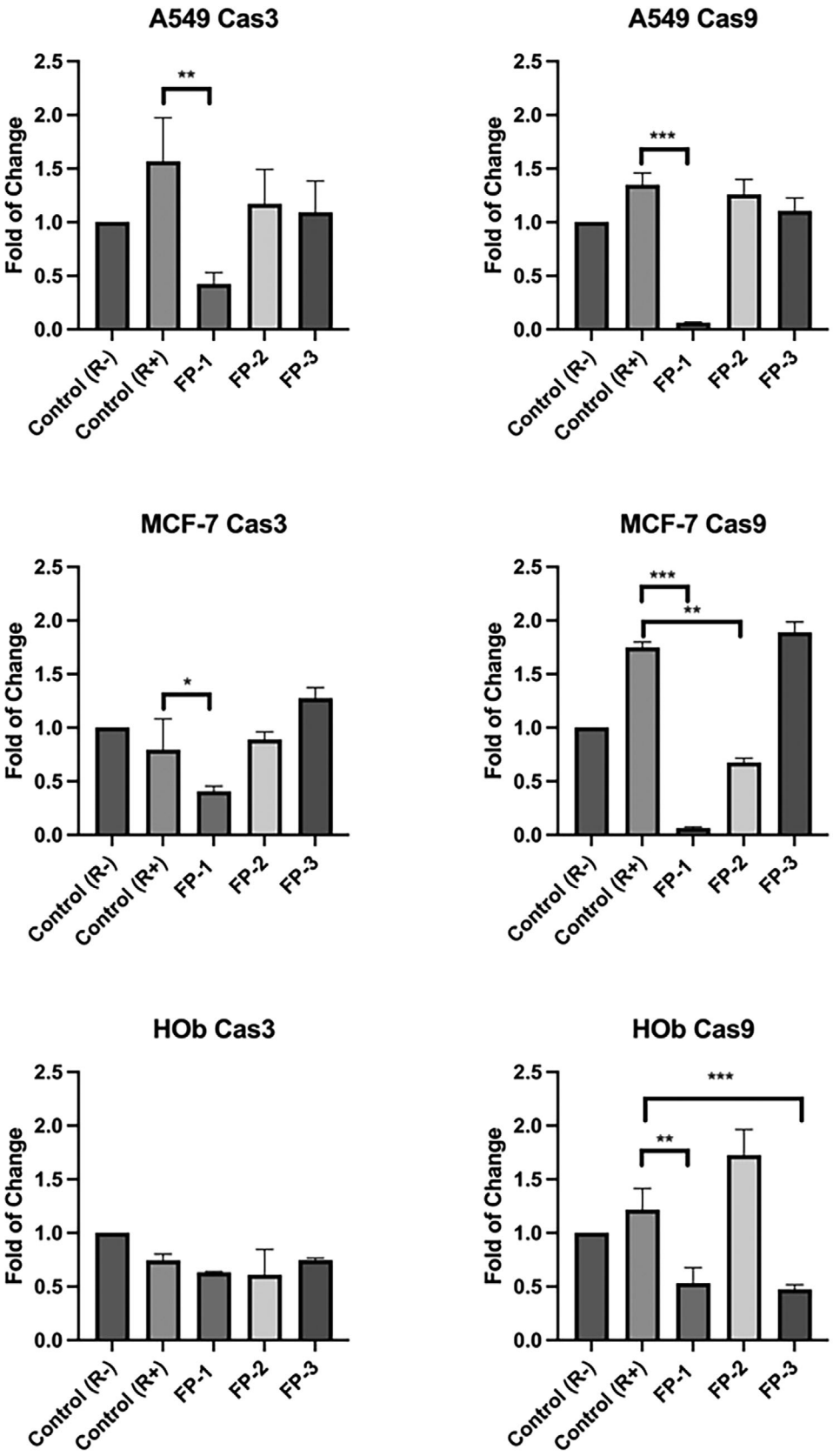

Figure 7. Expression levels of Caspase-3 and Caspase-9 genes in the A549, MCF-7, and HOb cell lines.

real-time tracking and visualization within cells. Research highlights the ability of these polymers to specifically target cancer cells, enhancing diagnostics and personalized treatment strategies. The structural attributes of the polymers, particularly those containing benzodithiophene units, contribute to their fluorescent properties and are indicative of their potential for rapid response in biological environments.

4. Determining Apoptosis via Gene Expression

Reverse Transcription Polymerase Chain Reaction (RT-PCR) is a fundamental molecular biology technique used in the analysis of genetic material, particularly in the conversion and amplification of RNA to DNA. This method first converts RNA to DNA in a step called reverse transcription and then produces millions of copies of this DNA through PCR. RT-PCR is frequently used in gene expression analyses to understand the activity levels of specific genes within an organism. This enables a deeper understanding of the molecular mechanisms of diseases, cellular responses, and genetic variations. Caspase 3 and Caspase 9 are proteins that play key roles in apoptosis (programmed cell death) and are thus critical for maintaining cellular homeostasis and preventing pathological conditions. In this study, cells were treated with niosomal cargos containing FP-1, FP-2, and FP-3, followed by radiotherapy experiments. Subsequently, total RNA was isolated from these cells to assess the expression levels of Caspase-3 and Caspase-9 genes. The results indicate that there were no statistically significant changes in the expression levels of Caspase-3 and Caspase-9 genes in cancer cell lines and the healthy cell line (**Figure 7**) compared to the radiotherapy-treated control group (Control +: refers to the group of cells that underwent radiotherapy; Control –: refers to group of cells that did not receive radiotherapy).

Radiotherapy can exert its effects on cells through various pathways, including DNA damage, hypoxia, proliferation, stem cell phenotype, and immune response.[60] In the literature, some studies indicate that radiotherapy demonstrates its efficacy through apoptosis,[61,62] while others suggest that its primary effect is through antiproliferation, effectively inhibiting cell proliferation without causing cell death.[63,64] Furthermore, Mukherjee & Chakraborty, (2019) suggest that these effects may be dose-dependent, with high doses causing cell loss and low doses exhibiting antiproliferative effects. The results of the study corroborate the efficacy of radiotherapy through its antiproliferative effects.[65]

5. Conclusion

This study comprehensively explored the synthesis, characterization, and application of fluorescent polymers (FP-1, FP-2, and FP-3) encapsulated within niosomal cargos for potential use in theranostic applications. Fluorescent nanoparticles and polymers have significantly advanced fluorescence imaging techniques, offering new dimensions to theranostic treatments. These fluorescent polymers provide the ability to conduct detailed cellular-level analyses, establishing them as crucial tools in biomedical research. Initially, niosomal cargos incorporating fluorescent polymers were formulated and characterized. Viability analyses conducted over 24, 48, and 72 h demonstrated that at certain doses, these cargos exhibit cytotoxic effects, and their potential to enhance radiotherapy was evaluated using a linear accelerator (LINAK) with 4 Gray of 6 MeV radiation. The fluorescence imaging capabilities of these polymers were also tested under a fluorescence microscope to ascertain their cellular uptake and localization. As a conclusion, fluorescent polymers, particularly those with conjugated π-electron systems, have shown promise in targeting cancer cells and monitoring treatment responses due to their unique properties and adaptability to biological systems. This study highlighted the potential of using fluorescent polymers and niosomal cargos in cancer treatment, demonstrating greater uptake in cancerous cells and supporting the antiproliferative effects of radiotherapy. The combination of advanced imaging techniques, radiotherapy, and novel fluorescent polymers underscores the importance of dose optimization to maximize therapeutic benefits while minimizing radiotherapy-induced adverse effects, thereby enhancing the overall efficacy of cancer treatments. To reach more definitive conclusions about this potential, future in vivo studies will provide further insights into the applicability of fluorescent polymers in theranostic applications.

Supporting Information

Supporting Information is available from the Wiley Online Library or from the author.

Acknowledgements

The author thanks TUSEB for their support (Project no: TUSEB A/2022-08-22411). Special thanks are also extended to Prof. Dr. Sadullah Ozturk from the Institute of Nanotechnology and Biotechnology at Istanbul University-Cerrahpasa for his valuable help. Open AI ChatGPT-4o was utilized as a language editting tool in the preparation of this publication.

Conflict of Interest

The authors declare no conflict of interest.

Data Availability Statement

The data that support the findings of this study are available from the corresponding author upon reasonable request.

Keywords

fluorescent polymers, niosomes, radiotherapy, theranostic treatment

Received: July 18, 2024
Revised: August 16, 2024
Published online: September 2, 2024

[1] H. Sung, J. Ferlay, R. L. Siegel, M. Laversanne, I. Soerjomataram, A. Jemal, F. Bray, *CA Cancer J. Clin.* **2021**, *71*, 209.
[2] L. Doganay, K. Ozdil, K. Memisoglu, S. Katrinli, E. Karakoc, E. Nikerel, G. D. Doganay, *North. Clin. Istanb* **2017**, *4*, 1.

[3] Y. Zhong, F. Meng, C. Deng, Z. Zhong, *Biomacromolecules* **2014**, *15*, 1955.
[4] M. J. Mitchell, M. M. Billingsley, R. M. Haley, M. E. Wechsler, N. A. Peppas, R. Langer, *Nat. Rev. Drug Discov.* **2020**, *20*, 101.
[5] R. Baskar, K. A. Lee, R. Yeo, K. W. Yeoh, *Int. J. Med. Sci.* **2012**, *9*, 193.
[6] X. Song, Z. Sun, L. Li, L. Zhou, S. Yuan, *Front. Oncol.* **2023**, *13*, 1088878.
[7] L. Barazzuol, R. P. Coppes, P. van Luijk, *Mol. Oncol.* **2020**, *14*, 1538.
[8] Z. Zhang, M. Lu, C. Chen, X. Tong, Y. Li, K. Yang, H. Lv, J. Xu, L. Qin, *Theranostics* **2021**, *11*, 3167.
[9] J. Lin, M. Yin, X. Liu, F. Meng, L. Luo, *Macromol. Rapid Commun.* **2022**, *43*, 2200194.
[10] E. Guler, H. Akbulut, C. Geyik, T. Yilmaz, Z. P. Gumus, F. B. Barlas, R. E. Ahan, D. O. Demirkol, S. Yamada, T. Endo, S. Timur, Y. Yagci, *Biomacromolecules* **2016**, *17*, 2399.
[11] G. Liberale, A. Bohlok, A. Bormans, F. Bouazza, M. G. Galdon, I. El Nakadi, P. Bourgeois, V. Donckier, *Eur. J. Surg. Oncol.* **2018**, *44*, 1301.
[12] D. Grosenick, C. Bremer, *Molecular Imaging in Oncology*, Recent Results in Cancer Research, Springer, Berlin, Germany **2020**, *216*, 591.
[13] Y. Chang, X. Meng, Y. Zhao, K. Li, B. Zhao, M. Zhu, Y. Li, X. Chen, J. Wang, *J. Colloid Interface Sci.* **2011**, *363*, 403.
[14] C. H. J. Choi, C. A. Alabi, P. Webster, M. E. Davis, *Proc. Natl. Acad. Sci.* **2010**, *107*, 1235.
[15] D. Cao, J. He, J. Xu, M. Zhang, L. Zhao, G. Duan, Y. Cao, R. Zhou, P. Ni, *Polym. Chem.* **2016**, *7*, 4198.
[16] S. Han, Y. Mu, Q. Zhu, Y. Gao, Z. Li, Q. Jin, W. Jin, *Anal. Bioanal. Chem.* **2012**, *403*, 1343.
[17] J. Klostergaard, C. E. Seeney, *Nanomedicine* **2012**, *1*, S37.
[18] P. Pericleous, M. Gazouli, A. Lyberopoulou, S. Rizos, N. Nikiteas, E. P. Efstathopoulos, *Int. J. Cancer* **2012**, *131*, 519.
[19] S. Liu, M. Wu, Z. Zhang, *Toxicol. Appl. Pharmacol.* **2010**, *246*, 163.
[20] C. Zhu, L. Liu, Q. Yang, F. Lv, S. Wang, *Chem. Rev.* **2012**, *112*, 4687.
[21] J. Jang, *Adv. Polym. Sci.* **2006**, *199*, 189.
[22] H. Yoon, M. Choi, K. J. Lee, J. Jang, *Macromol. Res.* **2008**, *16*, 85.
[23] H. Yoon, J. Jang, *Adv. Funct. Mater.* **2009**, *19*, 1567.
[24] G. L. Gibson, T. M. McCormick, D. S. Seferos, *J. Am. Chem. Soc.* **2012**, *134*, 539.
[25] A. Shimizu, Y. Ishizaki, S. Horiuchi, T. Hirose, K. Matsuda, H. Sato, J. I. Yoshida, *J. Org. Chem.* **2021**, *86*, 770.
[26] H. B. Mohamed, S. M. El-Shanawany, M. A. Hamad, M. Elsabahy, *Sci. Rep.* **2017**, *7*, 6340.
[27] M. Gharbavi, J. Amani, H. Kheiri-Manjili, H. Danafar, A. Sharafi, *Adv. Pharmacol. Pharm. Sci.* **2018**, *2018*, 6847971.
[28] L. Liu, W. Zhao, Q. Ma, Y. Gao, W. Wang, X. Zhang, Y. Dong, T. Zhang, Y. Liang, S. Han, J. Cao, X. Wang, W. Sun, H. Ma, Y. Sun, *Nanoscale Adv.* **2023**, *5*, 1527.
[29] R. Muzzalupo, L. Tavano, *Res. Rep. Transdermal Drug Delivery* **2015**, *2015*, 23.
[30] R. Khan, R. Irchhaiya, *J. Pharm. Invest.* **2016**, *46*, 195.
[31] S. T. Aslan, D. Cevher, E. Bolayır, G. Hizalan Ozsoy, Y. Arslan Udum, E. Yıldırım, L. Toppare, A. Cirpan, *Electrochim. Acta* **2021**, *398*, 139298.
[32] C. Y. Yu, C. C. Hsu, H. C. Weng, *RSC Adv.* **2018**, *8*, 12619.
[33] U. Bulut, S. Sanli, S. C. Cevher, A. Cirpan, S. Donmez, S. Timur, *J. Appl. Polym. Sci.* **2020**, *137*, 49332.
[34] A. Manosroi, P. Khanrin, W. Lohcharoenkal, R. G. Werner, F. Götz, W. Manosroi, J. Manosroi, *Int. J. Pharm.* **2010**, *392*, 304.
[35] L. Yin, Y. Li, J. Ren, H. Kuwahara, D. Kufe, *J. Biol. Chem.* **2003**, *278*, 35458.
[36] Y. Li, W. Wang, A. Li, W. Huang, S. Chen, F. Han, L. Wang, *Chem.-Biol. Interact.* **2021**, *1*, 109434.
[37] M. Erginer, B. Gökalsin, S. Tornaci, C. Sesal, E. T. Öner, *Int. J. Biol. Macromol.* **2023**, *240*, 124418.
[38] B. Carsten, F. He, H. J. Son, T. Xu, L. Yu, *Chem. Rev.* **2011**, *111*, 1493.
[39] H. Abd-El-Azim, A. Ramadan, N. Nafee, N. Khalafallah, *J. Liposome Res.* **2018**, *28*, 112.
[40] G. Chimote, R. Banerjee, *J. Biomed. Mater. Res., Part B* **2010**, *94*, 1.
[41] B. Demir, F. B. Barlas, E. Guler, P. Z. Gumus, M. Can, M. Yavuz, H. Coskunol, S. Timur, *RSC Adv.* **2014**, *4*, 34687.
[42] F. Nowroozi, A. Almasi, J. Javidi, A. Haeri, S. Dadashzadeh, *Iran. J. Pharm. Res.* **2018**, *17*, 1.
[43] N. Düzgüneş, S. Nir, *Adv. Drug Deliv. Rev.* **1999**, *40*, 3.
[44] J. Tang, M. Rakshit, H. M. Chua, A. Darwitan, L. T. H. Nguyen, A. Muktabar, S. Venkatraman, K. W. Ng, *Nanotechnology* **2021**, *32*, 505105.
[45] O. L. Ugorji, O. N. C. Umeh, C. O. Agubata, D. Adah, N. C. Obitte, A. Chukwu, *Heliyon* **2022**, *8*, e12369.
[46] H. A. M. Ardona, J. D. Tovar, *Bioconjug. Chem.* **2015**, *26*, 2290.
[47] C. Wu, B. Bull, C. Szymanski, K. Christensen, J. McNeill, *ACS Nano* **2008**, *2*, 2415.
[48] Z. Tian, J. Yu, C. Wu, C. Szymanski, J. McNeill, *Nanoscale* **2010**, *2*, 1999.
[49] K. Xu, F. Guidez, A. Glasow, D. Chung, K. Petrie, K. Stegmaier, K. K. Wang, J. Zhang, Y. Jing, A. Zelent, S. Waxman, *Cancer Res.* **2005**, *65*, 7856.
[50] T. Suzuki, O. Nagae, Y. Kato, H. Nakagawa, K. Fukuhara, N. Miyata, *J. Am. Chem. Soc.* **2005**, *127*, 11720.
[51] K. Chang, D. Gao, Q. Qi, Y. Liu, Z. Yuan, *Biomater. Sci.* **2019**, *7*, 1486.
[52] Y. H. Chao, S. C. Kuo, C. H. Wu, C. Y. Lee, A. Mauger, I. C. Sun, S. L. Morris-Natschke, K. H. Lee, *J. Med. Chem.* **1998**, *41*, 4658.
[53] Y. Jing, N. Hellinger, L. Xia, A. Monks, E. A. Sausville, A. Zelent, S. Waxman, *Cancer Res.* **2005**, *65*, 7847.
[54] H. Faghihi, M. R. Mozafari, A. Bumrungpert, H. Parsaei, S. V. Taheri, P. Mardani, F. M. Dehkharghani, M. Y. Pudza, M. Alavi, *Photodiagn. Photodyn. Ther.* **2023**, *42*, 103614.
[55] F. Ding, J. Feng, X. Zhang, J. Sun, C. Fan, Z. Ge, *Adv. Drug Deliv. Rev.* **2021**, *173*, 141.
[56] Y. H. Chan, P. J. Wu, *Part. Part. Syst. Charact.* **2015**, *32*, 11.
[57] D. Tuncel, H. V. Demir, *Nanoscale* **2010**, *2*, 484.
[58] W. Tan, T. Leng, G. Lai, Z. Li, J. Wu, Y. Shen, C. Wang, *Chin. J. Chem.* **2016**, *34*, 809.
[59] B. Keller, A. McLean, B. G. Kim, K. Chung, J. Kim, T. Goodson, *J. Phys. Chem. C* **2016**, *120*, 9088.
[60] J. M. Price, A. Prabhakaran, C. M. L. West, *Nat. Rev. Clin. Oncol.* **2023**, *20*, 83.
[61] Q. Huang, F. Li, X. Liu, W. Li, W. Shi, F. F. Liu, B. O'Sullivan, Z. He, Y. Peng, A. C. Tan, L. Zhou, J. Shen, G. Han, X. J. Wang, J. Thorburn, A. Thorburn, A. Jimeno, D. Raben, J. S. Bedford, C. Y. Li, *Nat. Med.* **2011**, *17*, 860.
[62] J. Cheng, S. He, M. Wang, L. Zhou, Z. Zhang, X. Feng, Y. Yu, J. Ma, C. Dai, S. Zhang, L. Sun, Y. Gong, Y. Wang, M. Zhao, Y. Luo, X. Liu, L. Tian, C. Li, Q. Huang, *Clin. Cancer Res.* **2019**, *25*, 3732.
[63] A. M. Shannon, K. J. Williams, *J. Pharm. Pharmacol.* **2008**, *60*, 1029.
[64] M. Widel, M. Widel, *Int. J. Med. Phys. Clin. Eng. Radiat. Oncol.* **2016**, *5*, 1.
[65] S. Mukherjee, A. Chakraborty, *Int. J. Radiat. Biol.* **2019**, *95*, 243.